AGU PUBLICATIONS

Global Biogeochemical Cycles

RESEARCH ARTICLE
10.1002/2016GB005493

Key Points:
- Shelf sediments of the northern Gulf of Alaska supply labile particulate Fe and dissolved Fe from wintertime sediment resuspension
- Concentrations of dissolved Fe are fairly constant over the shelf in late winter and in summer, perhaps regulated by organic ligands
- Modeling suggests that shelf sediments can supply Fe over the shelf, but that other Fe sources, including dust, are important offshore

Supporting Information:
- Supporting Information S1
- Figure S1
- Figure S2
- Figure S3
- Figure S4
- Movie S1
- Movie S2

Correspondence to:
J. Crusius,
jcrusius@usgs.gov

Citation:
Crusius, J., A. W. Schroth, J. A. Resing, J. Cullen, and R. W. Campbell (2017), Seasonal and spatial variabilities in northern Gulf of Alaska surface water iron concentrations driven by shelf sediment resuspension, glacial meltwater, a Yakutat eddy, and dust, *Global Biogeochem. Cycles*, *31*, doi:10.1002/2016GB005493.

Received 1 AUG 2016
Accepted 4 MAY 2017
Accepted article online 6 MAY 2017

Seasonal and spatial variabilities in northern Gulf of Alaska surface water iron concentrations driven by shelf sediment resuspension, glacial meltwater, a Yakutat eddy, and dust

John Crusius[1], Andrew W. Schroth[2], Joseph A. Resing[3], Jay Cullen[4], and Robert W. Campbell[5]

[1]USGS Alaska Science Center at UW School of Oceanography, Seattle, Washington, USA, [2]Department of Geology, University of Vermont, Burlington, Vermont, USA, [3]Joint Institute for the Study of the Atmosphere and the Ocean Pacific Marine Environmental Laboratory, University of Washington, Seattle, Washington, USA, [4]School of Earth and Ocean Sciences, University of Victoria, Victoria, British Columbia, Canada, [5]Prince William Sound Science Center, Cordova, Alaska, USA

Abstract Phytoplankton growth in the Gulf of Alaska (GoA) is limited by iron (Fe), yet Fe sources are poorly constrained. We examine the temporal and spatial distributions of Fe, and its sources in the GoA, based on data from three cruises carried out in 2010 from the Copper River (AK) mouth to beyond the shelf break. April data are the first to describe late winter Fe behavior before surface water nitrate depletion began. Sediment resuspension during winter and spring storms generated high "total dissolvable Fe" (TDFe) concentrations of ~1000 nmol kg^{-1} along the entire continental shelf, which decreased beyond the shelf break. In July, high TDFe concentrations were similar on the shelf, but more spatially variable, and driven by low-salinity glacial meltwater. Conversely, dissolved Fe (DFe) concentrations in surface waters were far lower and more seasonally consistent, ranging from ~4 nmol kg^{-1} in nearshore waters to ~0.6–1.5 nmol kg^{-1} seaward of the shelf break during April and July, despite dramatic depletion of nitrate over that period. The reasonably constant DFe concentrations are likely maintained during the year across the shelf by complexation by strong organic ligands, coupled with ample supply of labile particulate Fe. The April DFe data can be simulated using a simple numerical model that assumes a DFe flux from shelf sediments, horizontal transport by eddy diffusion, and removal by scavenging. Given how global change is altering many processes impacting the Fe cycle, additional studies are needed to examine controls on DFe in the Gulf of Alaska.

1. Introduction

Primary productivity in the Gulf of Alaska (GoA) is limited by availability of the micronutrient iron (Fe) [*Martin*, 1988; *Boyd et al.*, 2004]. Identifying and quantifying the Fe sources to this region are therefore of fundamental ecological importance. The northern GoA region has been understudied relative to many parts of the world's oceans, which has limited our understanding of key processes controlling the supply of Fe and other nutrients to surface waters there. Coastal waters in this region are often Fe-replete because of abundant Fe sources from rivers [*Schroth et al.*, 2011, 2014], shelf sediments [*Lippiatt et al.*, 2010; *Aguilar-Islas et al.*, 2016], and atmospheric inputs including dust [e.g., *Crusius et al.*, 2011], fossil fuel combustion [e.g., *Sholkovitz et al.*, 2009; *Schroth et al.*, 2009], and biomass burning [*Ito*, 2011]. However, we have a poor quantitative understanding of these Fe fluxes and of the complex set of processes that control Fe concentrations in surface waters, especially beyond the continental shelf break, where waters are known to be Fe-limited [e.g., *Boyd et al.*, 2004].

Much of the nutrient supply to surface waters in the GoA is derived from physical transport of deep waters to the surface, partly from convective and wind-driven winter mixing [*Bathen*, 1972; *Kara et al.*, 2000]. The deep north Pacific Ocean includes the oldest water along the meridional overturning circulation, which leads to high deepwater nitrate concentrations from organic matter respiration [e.g., *Whitney et al.*, 2013], aided by the long residence time of nitrate [*Brandes and Devol*, 2002]. In contrast to nitrate, Fe is sparingly soluble, particle-reactive, and is removed by scavenging, leading to its short residence time in deep waters of decades to a century [*Moore and Braucher*, 2008; *Bruland et al.*, 1994]. Deep water transported toward the surface therefore tends to be somewhat depleted in Fe compared to nitrate, relative to phytoplankton requirements. Thus, when upwelling or mixing is the dominant nutrient source to the euphotic zone, Fe tends to be the proximate limiting nutrient for photosynthetic algae. However, nitrate tends to be the limiting nutrient in

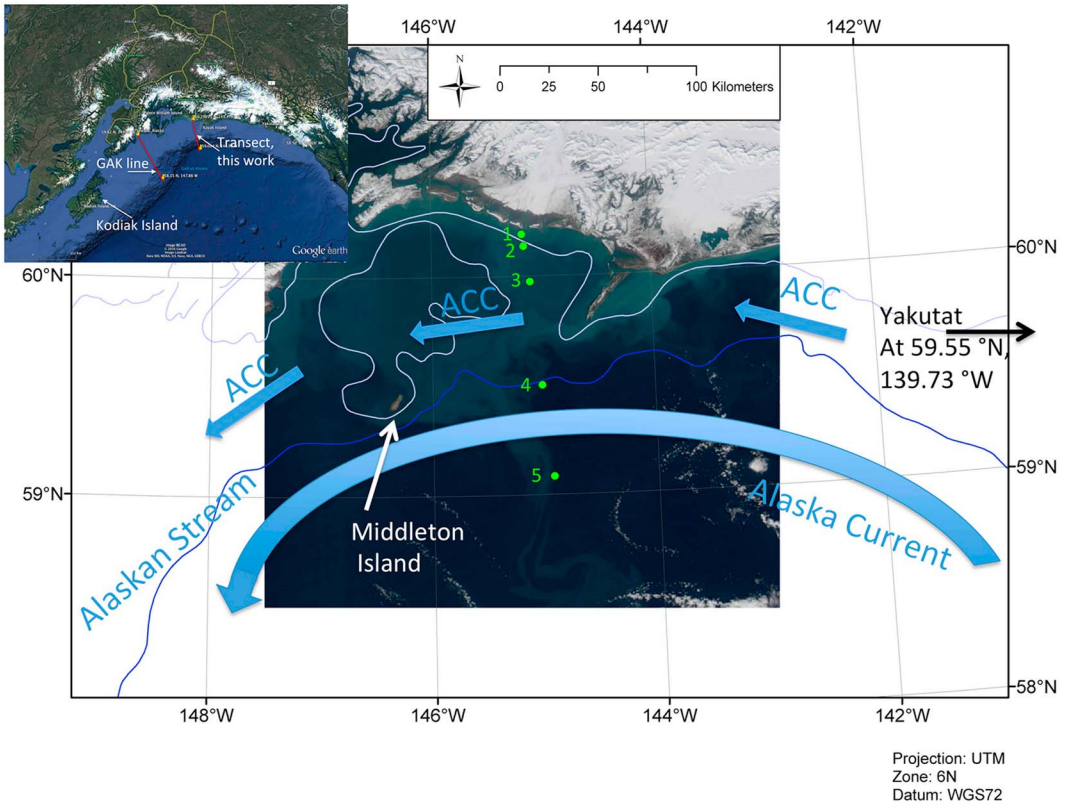

Figure 1. (top left) Expanded map of sampling region. The map at right shows the sampling stations (green circles) on the shelf/slope transect extending seaward from near the mouth of the Copper River (AK) (Station 1) to beyond the shelf break (Station 5). Surface water currents are denoted with blue arrows and include the Alaska Coastal Current (ACC) along the shelf, the Alaska Current, and Alaskan Stream [modified from *Lippiatt et al.*, 2011]. The thin blue contour line is the 500 m depth contour and gives the approximate position of the shelf break, while the white contour is the 100 m depth contour. Station locations and depth contours are superimposed on a MODIS true-color image from 9 April 2010, the same day Stations 4 and 5 were sampled. True-color image generated using HDFlook.

coastal waters of the northern GoA region [*Childers et al.*, 2005] because Fe is abundant, owing to terrestrial and marine sources. The importance of understanding mechanisms supplying both Fe and nitrate to surface waters in the region has been demonstrated by observations of high net community production and high CO_2 uptake in a coastal transition zone where surface waters rich in nitrate mix with waters rich in Fe [*Strom et al.*, 2006; *Palevsky et al.*, 2013]. Further justification stems from the observation that the catch of resident fish in this region is highest in coastal waters and has been tied to phytoplankton and zooplankton biomass [e.g., *Ware and Thomson*, 2005], which are likely linked to the supply of nutrients. Understanding the fundamental processes driving nutrient fluxes to surface waters in this region is made even more important by the fact that climate and global change are impacting many key processes, which could perturb the marine ecosystem in ways we do not understand.

While deep winter mixing offshore is an important source of nitrate to surface waters, deep winter mixing over the shelf can also supply Fe to surface waters by resuspension of shelf sediments that are rich in Fe. A portion of the Fe in resuspended sediments could dissolve or desorb from particles by nonreductive dissolution (see review in *Jeandel and Oelkers* [2015]), contributing to the pool of Fe available to phytoplankton. Despite the potential importance of this wintertime supply of Fe, there are only two published observations of water-column concentrations of Fe from coastal waters south of Alaska from nonsummer months. Both of these studies were carried out in May, one along the GAK line [Figure 1; *Wu et al.*, 2009] and the other further east, between Yakutat Bay and SE Alaska [*Aguilar-Islas et al.*, 2016].

The Fe fluxes from coastal waters toward open-ocean surface waters of the GoA are not well quantified, although many of the physical processes that lead to exchange between coastal and open-ocean waters

have been documented. While upwelling is a key process that could lead to offshore transport of coastal Fe-rich surface waters, this region of the northern GoA experiences downwelling during most of the year and only very infrequent upwelling [*Stabeno et al.*, 2004]. Another key mechanism of offshore Fe transport in the GoA is eddies, as they often form in Fe-rich coastal regions and transport coastally derived Fe offshore. While a number of other physical processes that could transport Fe offshore have been documented [e.g., *Stabeno et al.*, 2004; *Siedlecki et al.*, 2012], only a few such studies have actually included Fe observations [*Johnson et al.*, 2005; *Cullen et al.*, 2009; *Wu et al.*, 2009; *Lippiatt et al.*, 2011; *Brown et al.*, 2012; *Xiu et al.*, 2011; *Aguilar-Islas et al.*, 2016].

This paper helps to improve our understanding of Fe supply to GoA surface waters and transport offshore. We present late winter, spring, and summer conductivity-temperature-depth (CTD), nitrate, and Fe data from a northern GoA transect that extended from the mouth of the Copper River, across the continental shelf, and 50 km beyond the shelf break (Figure 1), examining possible controls on Fe concentrations. Much of the emphasis of this paper is on observations from April 2010, a time of year that is important because it sets the stage for and defines the conditions at the start of the phytoplankton blooms that ensue in the succeeding spring and summer months. Indeed, these April observations were made 1 month earlier in the year than any previous Fe measurements in the region and approximate winter conditions, because they predate biologically driven surface water depletion of nitrate. In April, we identify sediment resuspension as a source of labile particulate matter that is an important Fe source at that key time, and offshore transport by an eddy. We use a simple numerical model to show that a shelf sediment source can explain the late-winter supply of Fe over the shelf but that Fe concentrations diminish seaward of the shelf break. Observations from late July of 2010, in contrast, identify meltwater as the dominant source of Fe at that time, a source that is also confined close to the coast. Finally, calculations based on published dust flux estimates suggest that dust is likely one important source of Fe influencing the GoA well beyond the shelf break.

2. Methods

Three cruises were carried out along a transect in the northern GoA, extending from the mouth of the Copper River to ~50 km beyond the shelf break (Figure 1), from 7–9 April, 5–7 May, and 27–29 July of 2010. Surface waters were sampled by underway pumping of seawater through Teflon-lined tubing using a technique adapted from that of *Vink et al.* [2000], with the intake positioned a few centimeter forward from, and mounted to, a PVC towfish towed ~2 m below the surface. The towfish was suspended by a polyester line from a boom extending ~10 m from the starboard side of the ship to minimize contamination. Seawater was pumped using a shipboard air-operated Teflon-lined diaphragm pump to a shipboard clean lab, where both filtered and unfiltered samples were collected. Acropore cartridges (0.45 μm) were used to filter the surface water samples inline under N_2 pressure, without requiring any intermediate collection vessel, after flushing 10 L through each cartridge before first use. Surface water salinity, temperature, and sampling depth were logged once per minute using a YSI Sonde attached to the towfish. Samples below the surface were collected using 8 L externally closed Niskin bottles whose inner face was Teflon-coated, attached to Spectra (Dyneema) line, and triggered at depth using Teflon-lined messengers. Niskin bottles were processed in the shipboard clean lab within 3 h or less of sample collection. Acid-washed 0.45 μm Pall Supor filters were used in the clean lab to filter the seawater samples collected using Niskin bottles, also under N_2 pressure. All trace metal samples were stored double-bagged in acid-cleaned low-density polyethylene bottles and acidified to pH 1.8 in the shipboard clean lab with Seastar™ concentrated HCl within 3 days of collection, then stored for >6 months prior to analysis. "Total dissolvable" Fe concentrations (hereafter TDFe) were determined on the unfiltered samples by inductively coupled plasma–mass spectrometry (ICP-MS) using the Element 2 HR-ICP-MS at the Woods Hole Oceanographic Institution (WHOI) in medium-resolution mode following 20-fold or greater dilution, with Sc as an internal standard, and using NRC-Canada's SLRS-4 as a reference material. TDFe was also analyzed by Flow-Injection Analysis (FIA) at the Pacific Marine Environmental Laboratory, using the direct injection method of [*Measures et al.*, 1995]. Intercomparisons were carried out on ~40 samples, which agreed within 10%. We define "dissolved" Fe (hereafter DFe) as that which passed through one of the 0.45 μm filters described above. As is true of many Fe data sets, we did not distinguish between truly soluble Fe complexes and colloidal Fe composed of small particles that nonetheless pass through the filter. Therefore, what we call DFe is a mixture of colloidal and truly soluble Fe. While this is a limitation of

our approach, methods for evaluating both ligand concentrations and colloidal Fe are sufficiently novel and rare that state-of-the-art techniques do not always distinguish colloidal from ionic Fe with certainty [e.g., *Fitzsimmons et al.*, 2015]. We acknowledge that a better understanding of the partitioning among ionic, colloidal, and ligand-bound Fe is needed. DFe was determined by FIA at the University of Victoria using the method of *Obata et al.* [1993]. DFe concentrations were compared to the reference materials SAFe D1 (bottle number 254 of ~650 total) and SAFe D2. We measured a concentration of 0.57 ± 0.06 nmol kg^{-1} for SAFe D1, which agreed with the consensus values of 0.65 ± 0.1 that included lower concentrations among higher bottle numbers. For SAFe sample D2 we measured a concentration of 0.96 ± 0.04 nmol kg^{-1}, very close to the consensus value of 0.923 ± 0.029 nmol kg^{-1}. (http://www.geotraces.org/science/intercalibration/322-standards-and-reference-materials). For this work, only samples collected via underway pumping were analyzed for DFe, partly because of limited access to the required analytical facilities prior to 2016, and partly because of possible contamination of some surface water samples collected by Niskin bottle. Profiles of salinity, temperature, and fluorescence were measured with a Seabird SBE16 CTD, deployed at the same time as the collection of the subsurface water samples. All water column profiles were carried out to within roughly 5 m of the maximum water depth, except at station 5, where the water depth was ~4000 m. Macronutrient samples were filtered through a Whatman GF/F filter (nominal pore size 0.7 μm) and frozen within 15 min of filtration. Nitrate + nitrite concentrations were measured using the spectrophotometric method of *Jones* [1984] and were determined prior to and after the cadmium reduction step to account for nitrite in the samples. Absorbances were measured with a Varian CARY 50 spectrophotometer at 540 nm. Sea surface height deviation (SSHD) data were acquired from the AVISO program through the NOAA Coastwatch ERDDAP data server (product erdTAssh1day [*Ducet et al.*, 2000]).

3. Results and Discussion

We preface this section with a brief explanation of some terms used throughout this results section. The Copper River is the largest freshwater point source that drains into the Gulf of Alaska [*Wang et al.*, 2004]. As is typical for rivers along this mountainous coastline, discharge in the late spring and summer months is many times higher than at other times of the year, in response to increased snowmelt and melting of glaciers [see *Crusius et al.*, 2011, Figure 2; *Brabets*, 1997]. For the purpose of this paper, the terms "meltwater," "glacial meltwater," and "freshwater" are virtually synonymous in the summer and denote primarily discharge from rivers along the GoA coast. Glacial meltwater dominates supply of TDFe to the coastal GoA [*Lippiatt et al.*, 2010; *Schroth et al.*, 2011]. The term "Copper River Plume" denotes the lens of freshwater extending from the mouth of the Copper River that reaches its maximum extent in response to maximum discharge in the summer. Because the Copper River discharges ~15% of the freshwater discharge to the Gulf of Alaska [*Wang et al.*, 2004], the coastal Gulf may be more river-influenced at this location than elsewhere. In the winter and early spring, however, discharge from the Copper River is much lower, is not primarily meltwater driven [*Brabets*, 1997], and this work will show that it is a less important influence on the ocean at those times.

3.1. Winter Sediment Resuspension Drives Large Shelf-Wide Fe Flux

In April 2010, the mixed layer at stations 2–5 was 20–30 m deep (Figure 2) based on *Levitus* [1982] (a density increase of 0.125 kg m^{-3} from surface waters) and considerably shallower by the criteria of *Oka et al.* [2007] (a density difference of 0.03 kg m^{-3} from the surface). The maximum winter mixed layer depth was likely deeper, as it is typically ~100 m in the subarctic NE Pacific [*Oka et al.*, 2007]. This deep mixing led to resuspension of shelf sediments in the winter and early spring, clearly visible over the shelf in the Moderate Resolution Imaging Spectroradiometer (MODIS) satellite image from 9 April (Figures 1 and S1 in the supporting information), and manifested as very high concentrations of TDFe in surface waters sampled during both April and May (Figures 3 and 4). In April the surface water concentrations of TDFe were close to 1000 nmol kg^{-1} along much of the continental shelf, decreasing beyond the shelf break (Figure 3) by ~2 orders of magnitude compared to the nearshore stations. Vertical profiles were either well mixed with respect to TDFe or maintained surface maxima (Figure 4). TDFe concentrations were slightly lower in early May (Figures 3 and 4), perhaps because the water column was slightly more stratified (Figure 2).

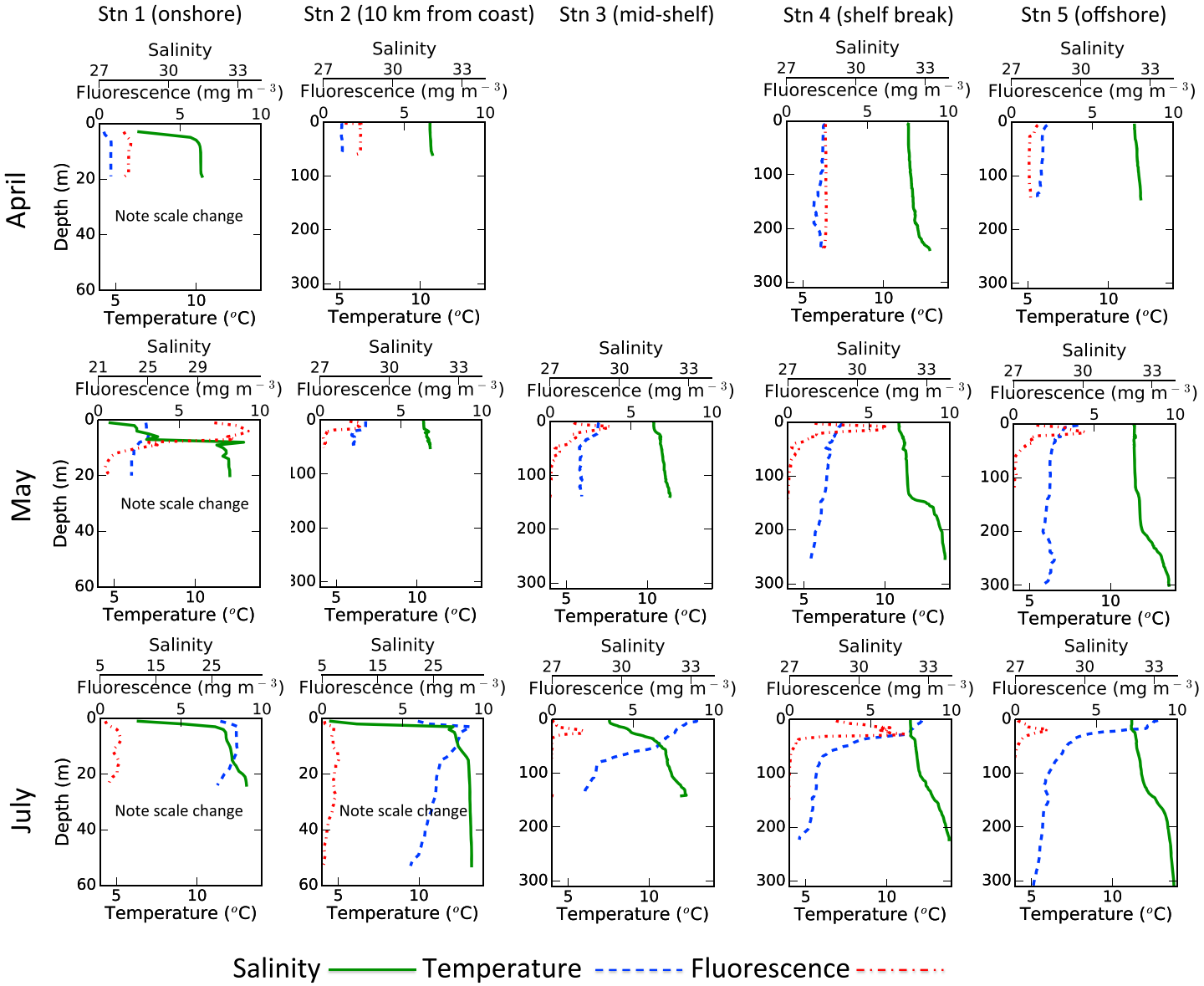

Figure 2. CTD profiles from early April, early May, and late July of 2010, showing salinity (green line), temperature (dashed blue line), and fluorescence (red dots and dashes) profiles at the five sampling stations shown in Figure 1. The scales are identical except for the salinity and depth scales of Station 1 and 2 closest to the coast. Water depth was roughly 5 m deeper than the maximum depth plotted, except at Station 5, where it was ~4000 m. The CTD profile did not extend as deep as normal at Station 5 in April because of an instrument malfunction.

These results collectively reveal that there was deep mixing and possibly tidal currents, in late winter and early spring, that led to sediment resuspension and extremely high concentrations of TDFe in shallow surface waters across most of the 80 km wide shelf. This suggests that sediment resuspension is an important source of TDFe along the continental shelf and beyond (and as we shall see later of DFe), at a time of critical ecological importance immediately prior to the spring bloom. Fairly constant surface water salinity of ~32 in surface waters (Figure 3) suggests only small fluxes of meltwater input in April, or in May, and that high particulate concentrations, as indicated by high TDFe concentrations to the shelf break and beyond, were not primarily caused by meltwater input at that time, but rather by resuspension of previously deposited sediment. These sediments that are resuspended from the shelf each winter are derived largely from summertime glacial discharge of massive quantities of meltwater and associated particles (glacial flour) to the coastal ocean [*Brabets*, 1997; *Schroth et al.*, 2011; *Schroth et al.*, 2014] . Indeed, the

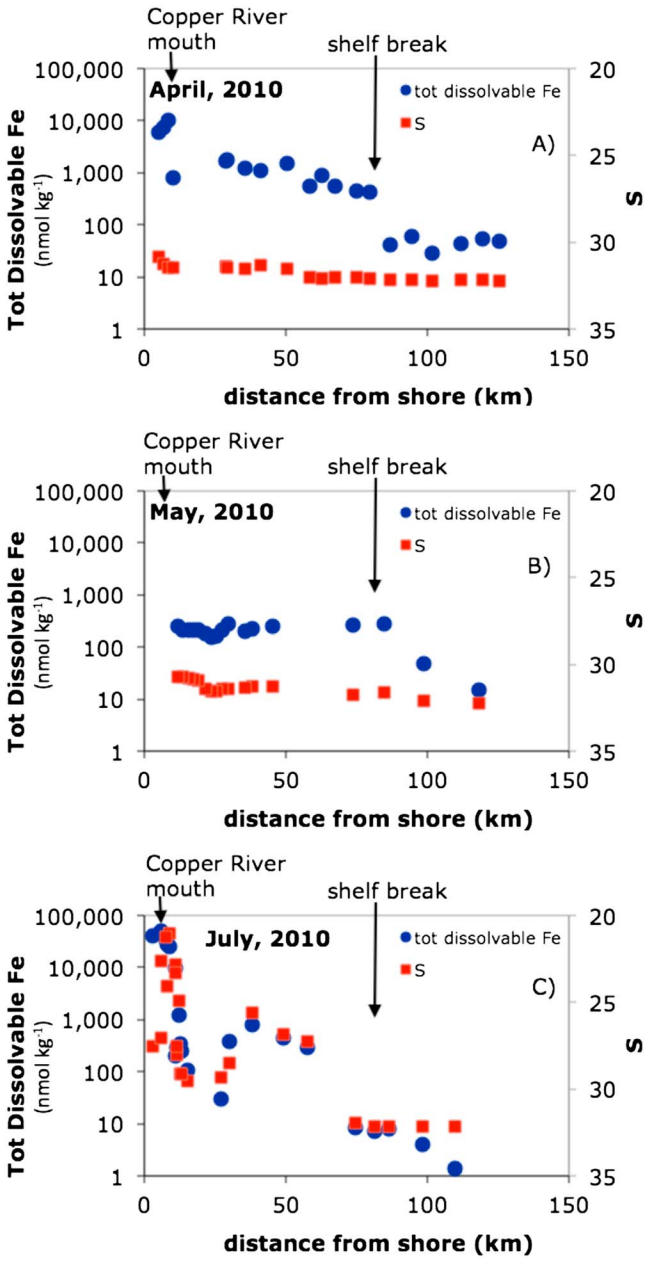

Figure 3. The surface water concentration of total dissolvable iron (TDFe; blue circles) and salinity (red squares), plotted versus distance from shore, along the sampling transect (Figure 1), in (a) April, (b) May, and (c) July of 2010.

sedimentation rates on the shelf in this region can exceed 2 cm a^{-1} in response to glacial weathering at high elevations of this mountainous region and are among the highest measured in the world [*Jaeger et al.*, 1998]. This large inventory of recently weathered sediments on the northern GoA shelf thus represents a large potential source of Fe to the coastal ocean. The shelf width at this location (80 km) is close to the average for the Gulf of Alaska coastline, with narrower shelves to the southeast and wider shelves to the southwest.

In late July of 2010 the water column was much more strongly stratified and spatially heterogeneous with respect to salinity and TDFe (Figures 2–4), owing to the tremendous amount of glacial meltwater discharged to coastal waters of the GoA [*Neal et al.*, 2010]. Surface water salinity was as low as ~10 (Figure 2) within the nearshore Copper River plume in response to high river discharge [e.g., *Brabets*, 1997]. Salinity increased to ~31 seaward of the river plume (Figure 3c), decreased to values as low as 25 between 30 and 60 km offshore in the Alaska Coastal Current [e.g., *Royer*, 1979] and increased to ~32 in the offshore stations (Figure 3c). Stratification was further enhanced by surface water warming. In July, surface water TDFe concentrations were inversely related to salinity on the shelf (Figure 3c). TDFe concentrations reached as high as tens of thousands of nmol kg^{-1} within the low-salinity Copper River plume, decreased seaward, then increased to concentrations of several hundred nmol kg^{-1} within the low-salinity Alaska Coastal Current (Figures 1 and 3), and decreased to as low as ~1 nmol kg^{-1} in the samples from farthest offshore. In July the controls on the high TDFe concentrations were entirely different than in April and May and were driven by input of meltwater (Figure 3), which included the Copper River plume itself, but also the waters of the Alaska Coastal Current (ACC), which is influenced by meltwater inputs from regions to the south and east of our sampling transect [*Royer*, 1982]. Surface water concentrations of TDFe were far lower near and seaward of the shelf break in late July, despite the large riverine inputs of TDFe, because there was neither a source of meltwater near the shelf break nor any process that could overcome the strong stratification to transport resuspended sediments from the seafloor to surface waters. It is worth noting that from the shelf break seaward, the highest surface water

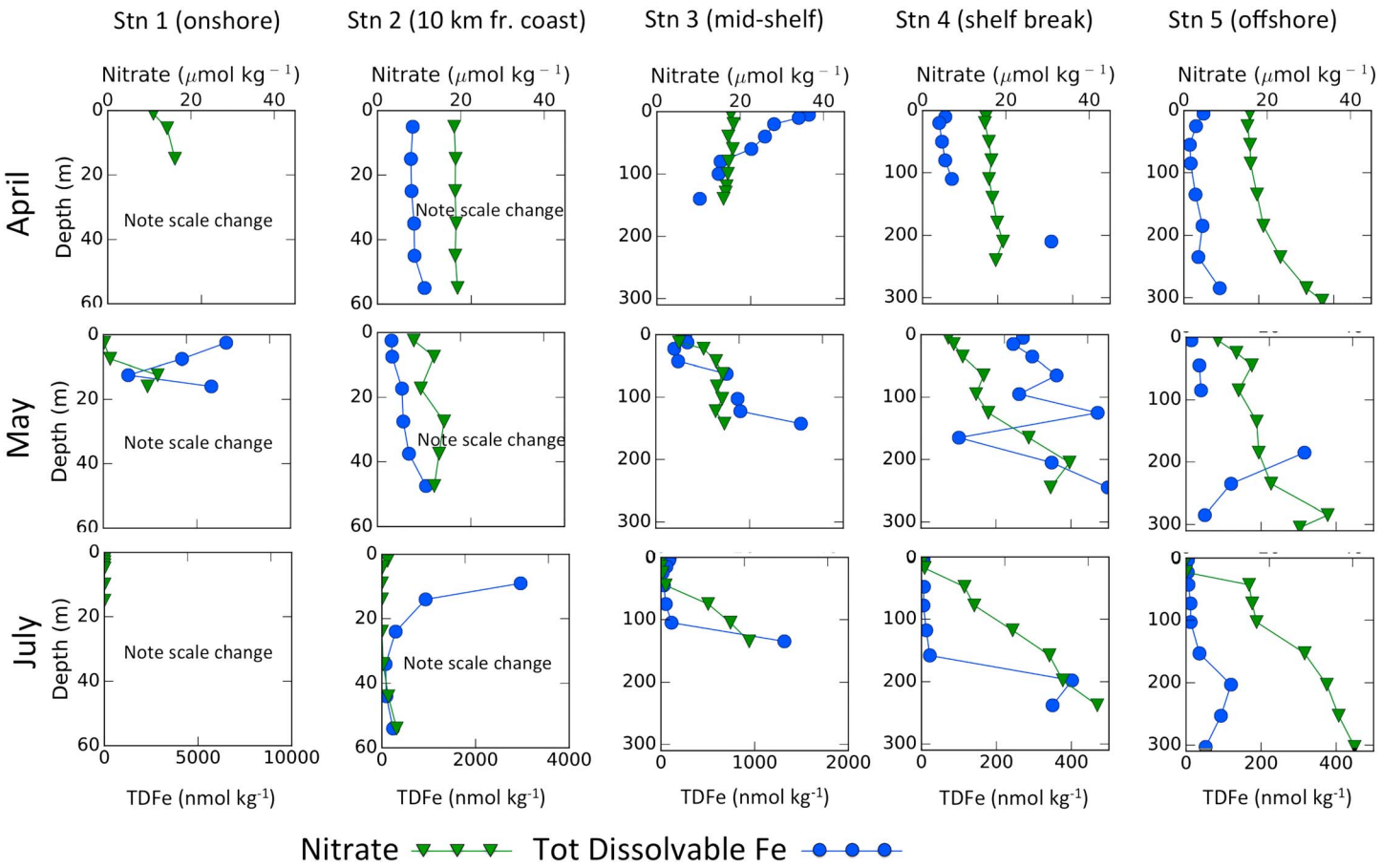

Figure 4. Nitrate (green triangles) and TDFe (blue circles) profiles. Nitrate scales are the same in each subplot but the TDFe scales change because of the large range. The depth scales of Stations 1 and 2 differ from the others. Sediment resuspension is manifest over the shelf in April and May as high TDFe concentrations also visible by satellite (Figures 1, 6b, and S1). Nitrate was well mixed in April yet partially depleted in May surface waters. In July surface waters, nitrate was fully depleted. TDFe concentrations were high in the Copper River Plume (see Figure 3) yet were low offshore of the plume, partly because biological processes removed Fe by uptake and by scavenging, and partly because stratification shut off supply from below. Some stations with anticipated high TDFe concentrations were not analyzed for fear of causing contamination of our analytical equipment (e.g., Station 1, April and July).

concentrations of TDFe of the year occur in response to sediment resuspension in winter and early spring (Figures 3a and 3b and 4), a time of minimal meltwater input.

3.2. Constant DFe Concentrations, Despite Variable TDFe and Nitrate Concentrations

Surface water DFe concentrations were fairly uniform across the shelf in both April and July (Figure 5), despite extremely large decreases in TDFe concentrations from the nearshore to offshore sampling sites (Figure 3). In April, DFe concentrations decreased from ~4 nmol kg^{-1} at the site closest to shore to ~1.5 nmol kg^{-1} at the most offshore site, while TDFe concentrations decreased from ~1000 nmol kg^{-1} to ~50 nmol kg^{-1} over the same distance. These DFe and TDFe concentrations are similar to observations from this region in May 2011 [*Aguilar-Islas et al.*, 2016]. In July, the highest DFe concentrations of ~10 nmol kg^{-1} were present in the low-salinity Copper River plume (Figures 3 and 5). These river-plume DFe concentrations are higher than the highest summer DFe concentrations of ~5 nmol kg^{-1} reported by *Aguilar-Islas et al.* [2016] from the northern GoA, but similar to the July nearshore concentration of "dissolved Fe" reported by *Wu et al.* [2009]. Given the similarity of the river-plume DFe concentrations reported in this work to the July DFe concentration of *Wu et al.* [2009] from their nearshore sample, it seems likely that the high river plume DFe concentrations reported here represent a short-lived transient signal of small colloids that would be expected to rapidly aggregate and settle out in response to estuarine mixing [see *Schroth et al.*, 2014]. These Copper River-plume DFe concentrations are consistent, furthermore, with DFe concentrations collected within the fresh water portion of

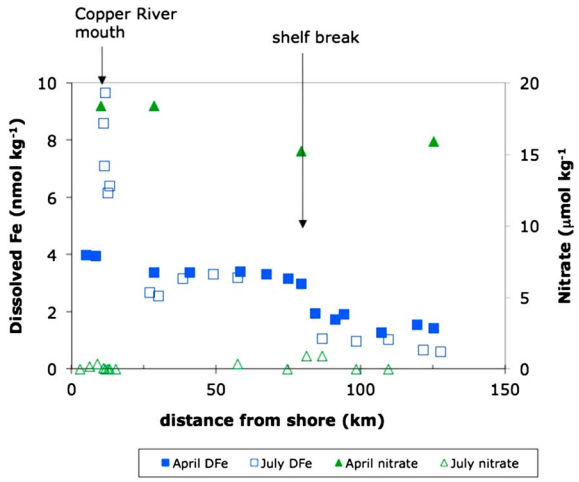

Figure 5. Surface water dissolved Fe concentrations in April (solid blue squares) and July (open blue squares, and nitrate concentrations in April (solid green triangles) and July (open green triangles), plotted versus distance from shore. The approximate location of the shelf break is denoted by an arrow. Note that dissolved Fe concentrations vary only a small amount between April and July along this transect, in contrast to nitrate concentrations and total dissolvable Fe concentrations (Figures 3 and 4).

the Copper River, of several tens of nmol kg^{-1} to over hundreds of nmol kg^{-1} [*Lippiatt et al.*, 2010; *Schroth et al.*, 2014]. Seaward of the river plume, the DFe concentrations over the shelf in July were close to ~3 nmol kg^{-1}, similar to the concentrations in April (Figure 5), and they decreased to values of ~0.5 nmol kg^{-1} at the most seaward portions of the transect. Between April and July, surface water nitrate became depleted (Figures 4 and 5), TDFe concentrations decreased by at least an order of magnitude (Figures 3 and 4), yet DFe concentrations remained remarkably constant (Figure 5). Lack of depletion of DFe suggests that some process is acting to control (regulate) surface water DFe concentrations over the shelf and slope, most likely strong Fe-complexing organic ligands, as first suggested by *Lippiatt et al.* [2010]. This suggestion is supported by concentrations of strong Fe-complexing ligands (log $k_1 \geq 12.0$) observed in spring of ~1–4 nmol kg^{-1} in the northern coastal GoA region that are only slightly higher than DFe concentrations measured on the same samples [*Aguilar-Islas et al.*, 2016]. The relatively constant DFe concentrations over the shelf in April and July despite enormous differences in TDFe concentrations (Figures 3–5), coupled with the similarity of these DFe concentrations to other published DFe concentrations from the northern GoA shelf [*Lippiatt et al.*, 2010; *Aguilar-Islas et al.*, 2016], and the similarity of springtime DFe concentrations to concentrations of strong ligand concentrations wherever they have been measured in this vicinity [*Aguilar-Islas et al.*, 2016] suggest that DFe may be dominated by ligand-bound Fe. This ligand-bound Fe fraction may constitute an organic colloidal fraction, although an inorganic colloidal Fe fraction is probably also present, given the high TDFe concentrations caused by fine-grained glacial flour at all sampling times.

3.3. Inferring the Nitrate:DFe and Fe:C Uptake Ratios

In April, when surface waters were nitrate-replete, the nitrate: DFe ratio ranged from ~5000 at the station closest to the coast, to ~11,000 at the most offshore site. If both DFe and nitrate were completely taken up, and we assumed a Redfield ratio of C:N of 106:16, this would have allowed an Fe:C uptake ratio of 30 μmol mol^{-1} at the nearshore site and ~13 μmol mol^{-1} at the most offshore site. These are very plausible values for the Fe:C uptake ratio, typical of luxury Fe uptake by coastal diatoms close to shore and lower Fe uptake beyond the shelf break, where Fe supply is reduced [e.g., *Sunda and Huntsman*, 1995; *Marchetti et al.*, 2006]. Indeed, the spring bloom in this region has been observed to be dominated by diatoms [*Strom et al.*, 2016], with communities varying across the shelf [*Strom et al.*, 2006]. However, by late July, the surface water nitrate concentration was fully depleted (Figures 4 and 5), whereas the DFe concentrations were either similar to or only slightly diminished compared to the April concentrations. The DFe concentrations are most likely maintained at fairly constant concentrations from April through July over the shelf as a result of the high particulate Fe concentrations sustained by sediment resuspension in the winter and spring, and by meltwater in the summer (Figures 3 and 5), together with solubilization of the particulate Fe by the Fe-complexing ligands, despite likely DFe uptake by phytoplankton implied by the nitrate depletion. This observation of the continued release of DFe from resuspended coastal sediments would not have been possible without obtaining both the winter and summer data. Note that the presence of colloidal Fe species may have influenced biological availability of Fe, although the nitrate depletion from surface waters between April and July indicates clearly that Fe was utilized by phytoplankton.

3.4. Offshore Fe Transport by a Yakutat Eddy

The impact of coastal Fe sources on DFe concentrations in the open ocean is not well understood and is influenced by the processes that transport coastal waters offshore; eddies are one such process. By convention, these eddies have been given names based on their site of formation including Haida [*Crawford*, 2002], Sitka [*Tabata*, 1982], Yakutat [*Ladd et al.*, 2005a] and Kenai eddies [*Rovegno et al.*, 2009]. Previous studies have shown that Haida eddies capture Fe in their coastal waters of origin and transport that Fe westward, toward the open ocean [*Johnson et al.*, 2005; *Xiu et al.*, 2011]. The Yakutat eddies [*Ladd et al.*, 2005a] are confined by the coastline and travel approximately westward along the shelf break, typically reaching the Kodiak Island region (Figure 1) in 4–12 months [*Okkonen et al.*, 2003]. The anticyclonic (clockwise-rotating) Yakutat eddies therefore have an additional impact on offshore transport of Fe that Haida eddies do not have, in that they induce exchange of seawater across the continental shelf. Slope waters are advected onto the shelf along the west flank of the eddies, and shelf waters are advected offshore along their east flank. These physical influences of Yakutat eddies have been described elsewhere [*Gower and Tabata*, 1993; *Okkonen et al.*, 2003; *Ladd et al.*, 2005a; *Crawford et al.*, 2007]. However, the Fe data presented in this paper are the first, to our knowledge, from within a Yakutat Eddy as it traveled westward during the early spring, thereby capturing some of the impact of this surface water advection on particulate and dissolved Fe. We present these data below, recognizing that this study merely captured one of these eddies as it transited and was not designed to fully characterize the eddy and its impacts.

An eddy formed near Yakutat (AK) by February of 2010, visible as a ring of water ~100 km in diameter characterized by a sea surface height deviation greater than of 0.15 m, traveling ~westward along the shelf break and reaching our sampling transect in late March (Figure 6a). The trajectory of this eddy can be viewed as a time series in Movies S1 and S2 in the supporting information. In mid-March the eddy was positioned such that our sampling transect was along the western flank. This position suggests that basin water was transported onto the shelf along our transect at that time (Figure 6a). By early April the eddy had moved westward such that the eastern eddy flank was along our transect. This should have caused offshore (southward) transport of shelf water beyond the shelf break at that time.

The recent offshore transport of particulate matter beyond the shelf break is clearly visible in the MODIS true-color image from 9 April, as an ~15 km wide high-particle region extending perpendicular to and more than 80 km beyond the shelf break, approaching Station 5 (Figures 1 and 6b). This feature can be most clearly seen in Figure S1. The position of this particle-rich feature is entirely consistent with the documented location of the anticyclonic Yakutat eddy on 7 April (Figures 6a and 6b and S1), which would be predicted to induce clockwise flow and therefore offshore advection along its eastern flank.

Previous observations of Yakutat eddies [*Ladd et al.*, 2005b] have inferred a maximum current velocity of ~0.4 m s^{-1} (~35 km d^{-1}). If we assume surface current speed averaged half of this value along the trailing (eastern) edge of the Yakutat eddy in early April, these high-Fe waters would have traversed half of the shelf in 2 days (Figures 1 and 6). If the diameter of the Yakutat eddy is ~100 km (Figures 6a and 6b), and the center of the eddy is at the shelf break, the effect of this Yakutat eddy as it passes westward along the shelf break, during winter and spring, would be to rapidly advect resuspended sediments, and associated Fe-enriched surface waters, ~50 km beyond the shelf break, roughly consistent with our April observations (Figures 1, 3, 6b, and S1). This offshore advection of particles is manifest as surface water TDFe maxima at the most offshore station 5, also from 9 April, caused by advection of very high TDFe surface waters from the shelf (Figures 3 and 4). The surface water TDFe concentrations are ~50 nmol kg^{-1} at Station 5 on 9 April, roughly 50 times higher than the DFe concentration, 50 km seaward of any possible shelf source, and far higher than at other times at this station (Figures 3 and 4).

Assuming that these resuspended particles would sink rapidly from surface waters in the absence of eddy-induced advection, the Yakutat Eddy can be thought of as effectively expanding the width of the shelf, or the spatial extent of surface waters which experience these high concentrations of suspended particulate matter from this source. This was discussed theoretically, without direct evidence, in *Ladd et al.* [2005a, 2005b] and in *Crawford et al.* [2007]. Kenai eddies are also confined by the coast and therefore travel approximately westward along the shelf break [*Rovegno et al.*, 2009], behavior that has also been occasionally observed for Sitka eddies [*Crawford et al.*, 2000]. Therefore, any such eddies transported along the shelf break could transport resuspended particles offshore as described here for the Yakutat eddy.

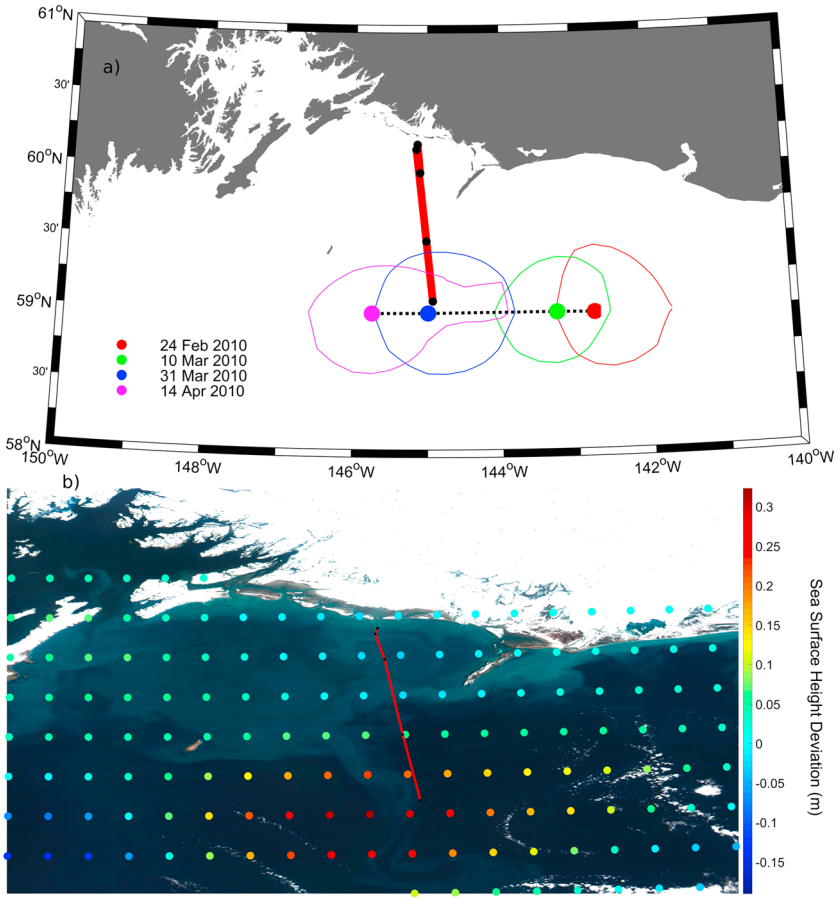

Figure 6. Evidence for a Yakutat eddy moving westward along the northern GoA shelf break. (a) Time series of 0.15 m sea surface height deviation (SSHD) contours from late February to mid-April 2010. The center of the eddy on each day is denoted with a dot and has been estimated as the point of maximum SSHD, estimated by linear interpolation. (b) MODIS true-color image from 9 April 2010 (Aqua satellite). Superimposed are sea surface height data from 7 April 2010 revealing a "Yakutat" eddy, apparent as a sea surface height deviation of ~0.3 m centered west and slightly south of the offshore edge of our sampling transect (red line; the black dots along the line represent Stations 1 (nearshore) through 5 (farthest offshore)). These eddies are anticyclonic, meaning they rotate clockwise in the northern hemisphere. At the time of these images, there would have been offshore advection along the eastern flank of the eddy. This behavior of the eddy is further manifested as particles visible as a 15 km wide band of light blue color beyond the shelf break (see Figures 1 and S1) and as surface TDFe maxima in the most offshore samples (Figure 4).

The evidence provided earlier that resuspension of shelf sediments drives high DFe concentration over the shelf supports the concept of *Chase et al.* [2007] that shelf sediments serve as a "capacitor" that regulates Fe supply to offshore waters. The observation that this Yakutat eddy advects resuspended sediments to surface waters well beyond the shelf break (Figures 4, 6b, and S1) extends this concept, suggesting that offshore transport processes, including any eddy that propagates westward along the shelf break, can transport high-Fe waters by as much as ~50 km or more beyond the shelf break during winter and early spring, when high concentrations of resuspended sediment are common over the shelf. These eddies also transport nitrate along their eastern flank toward coastal waters, which are nitrate-limited [e.g., *Childers et al.*, 2005]. This eddy-enhanced transport may augment the nutrient supply to the entire coastal region and help to explain, along with other mechanisms, why these coastal waters are highly productive [e.g., *Ware and Thomson*, 2005; *Palevsky et al.*, 2013], despite downwelling conditions much of the year [e.g., *Stabeno et al.*, 2004].

3.5. Comparison of TDFe and DFe Data to Other High-Latitude Regions

We can better place these data in context by comparing the behavior of both TDFe and DFe in this coastal Alaska setting to data from the coastal Southern Ocean and Greenland, other high-latitude sites where Fe

sources also include meltwater and shelf sediments. While it would be useful to compare quantitative models of Fe transport, very few studies of high-resolution coastal Fe data are interpreted with such models. One simple comparison that has often been made is of the distance over which TDFe and DFe concentrations decrease offshore, which could give some measure of the potential importance of coastal Fe sources to offshore waters. *Johnson et al.* [1997] defined the "scale length" as the distance over which the TDFe or DFe concentration decreases from a coastal maximum to a concentration some distance offshore equal to 1/e (0.37) times the maximum concentration. While easy to estimate, the scale length concept does not factor in the processes that drive seasonal and spatial variabilities in TDFe and DFe concentrations in this work, including sediment resuspension, physical mixing, meltwater inputs, eddies, and possibly complexation by organic ligands, which in turn lead to TDFe and DFe concentrations that do not decrease monotonically offshore. However, we will estimate scale length for comparison, as the data allow, and follow up with more complex modeling later.

The surface water TDFe concentrations from April decreased with a scale length of 23 km, as defined by the entire transect (r^2 = 0.86; Figure 3a). The DFe concentrations in this work were fairly constant over the shelf and decreased beyond the shelf break. We therefore estimate a DFe scale length from the distance beyond the shelf break over which the DFe concentration decreased to 1/e times the typical shelf concentration (3.4 nmol kg^{-1}). The April DFe scale length is ~30–70 km, depending on how we fit the DFe data. Scale length estimates based on May 2004 DFe and TDFe data from the GAK line (Figure 1) [*Wu et al.*, 2009] are at least 20% greater than our estimates, taken simply at face value. However, samples were not collected at fine enough spatial resolution to permit a definitive comparison.

These scale length estimates from surface waters from this work are intermediate values compared to other estimates. Off the Antarctic Peninsula, *Ardelan et al.* [2010] estimated a scale length of 12 km for TDFe and 25 km for DFe. Off Pine Island glacier in the Amundsen Sea (Southern Ocean; the TDFe scale length was estimated to be 62.5 km, while the scale length for DFe was 39 km [*Gerringa et al.*, 2012], offshore of the Kerguelen Islands (S. Ocean)), the DFe scale length was 151 km [*Bucciarelli et al.*, 2001]. A far more thorough review is presented in *Hopwood et al.* [2015].

The scale lengths estimated in this work are estimated for April and are driven entirely by physical processes, because nitrate concentrations remained near their winter maxima at that time (Figure 4), meaning biological processes were not yet leading to a decrease in surface water DFe concentrations. By contrast, the scale lengths estimated for some studies do not consider the possible impact of the season on their estimate, despite surface water DFe residence times that can be less than 1 week in some settings owing to biological uptake [*Dulaiova et al.*, 2009; *Ardelan et al.*, 2010], and are often less than 1 year [*Moore and Braucher*, 2008]. Some previous studies with comparatively long scale lengths (~100–150 km for DFe) were based on spring sampling, when the offshore DFe concentrations were not yet drawn down as much by biological processes [*Wu and Luther*, 1996; *Bucciarelli et al.*, 2001]. The DFe scale length estimates for this Southern Alaska site are only a factor of 2 shorter than the longest scale lengths reported to date [*Wu and Luther*, 1996; *Bucciarelli et al.*, 2001], despite the presence of strong alongshore currents along the Southern Alaska coast, which have been suggested in previous studies to reduce offshore Fe transport and cause much shorter scale lengths [*Hopwood et al.*, 2015].

3.6. Modeling Wintertime Fe Supply and Transport Beyond the Shelf

The water-column sampling carried out in April of 2010 occurred before any significant phytoplankton bloom had occurred that spring, based on the elevated nitrate concentrations at that time (Figures 4 and 5). The concentrations of DFe observed across the continental shelf were nearly constant at that time, and they decreased almost immediately beyond the shelf break (Figure 5). Because we can ignore biological processes and their impacts on DFe at this time of year, and because the water column (and TDFe concentrations) was reasonably well mixed in the vertical (Figures 2 and 4), we use a simple time-dependent 1-D numerical model to examine possible controls on the DFe concentrations. This offers a more process-driven evaluation of DFe data than the evaluation of removal scale length. We recognize that processes cannot truly be interpreted as one dimensional, especially given strong alongshore currents (Figure 1), but the one-dimensional approximation is reasonable if waters advecting into the region are similar to the waters they displace. The one-dimensional model is also justified by the observed surface maxima in TDFe along the sampled transect in April of 2010, suggesting that processes in surface waters are largely driving surface water TDFe and DFe

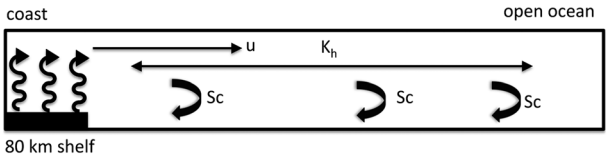

Figure 7. Schematic of the processes described by the 1-D dissolved Fe (DFe) supply and transport model used in this work. The model includes a DFe flux from shelf sediments, horizontal mixing by eddy diffusion, and DFe removal by first-order scavenging. The continental shelf is assumed to be 80 km wide. The winter mixed layer is assumed to be 100 m deep. The water column is specified to be wide enough (on the order of 1000 km) that the DFe concentration decreases to zero at the offshore boundary. The shelf sediment DFe flux is assumed to driven by the combined processes of sediment resuspension and dissolution of Fe from these particles, expressed as a simple DFe flux (nmol Dfe m^{-2} d^{-1}) over the entire shelf. An initial DFe concentration of 3.4 nmol kg^{-1} is assumed over the shelf, and the maximum dFe concentration allowed is set by a specified concentration of strong DFe-complexing ligands, also assumed to be 3.4 nmol kg^{-1}. The horizontal eddy diffusion coefficient (K_h) and the first-order scavenging rate constant (Sc) are variable parameters. The model allows for horizontal advection (μ), although this feature was not used to fit the observed DFe data (see Figure 8).

concentrations at that time. We use this simple model as a tool to demonstrate that late-winter shelf and slope surface water DFe concentrations can be simulated reasonably well assuming that shelf sediments are the only DFe source, with DFe removal by scavenging, with the result that the shelf-derived DFe supply is largely confined within a couple of hundred kilometers of the continental shelf break. We also use the model to help identify future observations needed to improve both our understanding and future Fe models.

The transport of dissolved Fe from the coast can be approximated in this case by a one-dimensional advection-diffusion-reaction equation where

$$\frac{\partial \mathrm{DFe}}{\partial t} = \frac{\partial}{\partial x} K_h \left[\frac{\partial [\mathrm{DFe}]}{\partial x}\right] - u\left(\frac{\partial [\mathrm{DFe}]}{\partial x}\right) - Sc\cdot[\mathrm{DFe}]$$

where [DFe] = concentration of dissolved Fe (nmol kg^{-1}).

x = distance from shore (m)
t = time (d)
K_h = horizontal eddy diffusivity (m^2 s^{-1})
u = horizontal current velocity (m s^{-1})
Sc = scavenging rate constant (d^{-1})

For simplicity we leave out unit conversions.

The numerical model used to interpret the surface water DFe data is adapted from *Crusius* [1992] and is written in the C programming language. The initial condition assumes a certain concentration of DFe over the shelf, which is 80 km wide. Boundary conditions include that Dfe ➔ 0 as x ➔ ∞. The depth of the modeled "surface water" box was assumed to be 100 m for these model runs. The typical water column width was ~2000 km, with a typical model grid spacing of 0.25 km. The typical time step for the model runs was 0.001 day (~1 min). The processes simulated by the model are presented schematically in Figure 7. Note that the model considers only "dissolved" Fe (what passes through a 0.45 μm filter; see section 2) and does not distinguish between colloidal and soluble inorganic and organic Fe complexes, nor do most DFe data sets. A concentration of strong ligand (L1) of 3.4 nmol kg^{-1} is assumed for the entire water column whose only role in the model is to limit the maximum allowable DFe concentration, above which any DFe is removed (probably by scavenging, although the process is not formally defined in the model). This has also been hypothesized by *Lippiatt et al.* [2010] and is reasonably consistent with the scant data available on Fe-binding ligand concentrations and binding strength (log $k_1 \geq 12.0$) in the northern GoA region (ligand source unknown [*Aguilar-Islas et al.*, 2016]). The only iron source that is modeled is shelf sediments. A DFe flux from the shelf sediments is specified, and the concentration of DFe can increase over time in response, up to the upper limit equal to the concentration of strong Fe-binding ligands. The process by which the DFe flux is released from sediments is not specified, although it could reasonably be driven by the documented sediment resuspension that leads to high particulate concentrations in shelf surface waters, coupled with nonreductive dissolution of a small fraction of that particulate Fe, as has been suggested to be important in many

Table 1. Model Parameters Used in Simple 1-D Model Simulations of April 2010 Dissolved Fe Concentrations (Figure 8)[a]

Model Parameter	Best Fit Range	Comments	Reference
Sedflux (nmol Fe m^{-2} d^{-1})	>5000	High flux fits high Sc. Low flux fits low Sc.	[*De Jong et al.*, 2015]
Horizontal eddy diffusivity, K_h (m^2 s^{-1})	180–360	Scaled for nearshore region.	[*Okubo*, 1971; *De Jong et al.*, 2015]
Scavenging rate constant, Sc (d^{-1})	0.003–0.016	Lowest Sc can fit if we assume lower sedflux. Higher Sc required if higher sedflux assumed.	[*Moore and Braucher*, 2008]

[a]See section 3.6 and Figure 7.

locations [*Jeandel and Oelkers*, 2015]. Particles are not modeled directly. Horizontal mixing is driven by the assumed horizontal eddy diffusivity. The model also allows for horizontal advection. DFe removal is driven by chemical scavenging, which is modeled as a simple first-order process with a uniform rate constant that is independent of particle concentration. This represents net scavenging removal. This is very similar to the scavenging treatment invoked by many more sophisticated Fe models [e.g., *Moore and Braucher*, 2008; *Nickelsen et al.*, 2015]. The numerical model results were validated by comparison to a steady state analytical solution in Figure S2. For simplicity, these time-dependent model runs were carried out using time-independent parameter values, for a total of 150 model days, to simulate processes occurring over the winter, e.g., from early November to early April, the time of our earliest sampling. We point out that there is no unique model fit to these data. For example, an increased Fe source from sediments could be counterbalanced by a higher horizontal diffusivity or by a higher Fe scavenging rate constant. The model is run with parameter values derived from other studies simply to test whether the DFe observations are consistent with a shelf Fe source. Values for all model parameters are listed in Table 1 and Figure 8. Additional model details are provided in the supporting information.

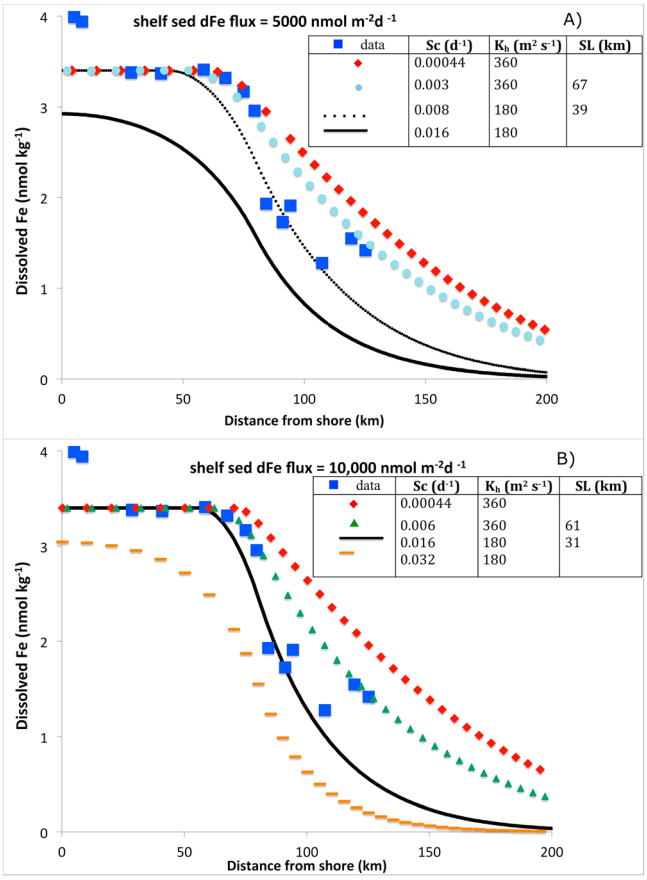

Figure 8. Model simulations of surface water DFe concentrations from the northern GoA shelf and slope region. The data can be fit reasonably well using a 1-D model that considers the DFe flux only from shelf sediments of (a) 5000 nmol m^{-2} d^{-1} or (b) 10,000 nmol m^{-2} d^{-1}, horizontal eddy diffusion, and removal by first-order scavenging. Constant rates of modeled processes are assumed for each 150 day long model run. The values for the parameters are all within the range of previous models, as summarized in Table 1. "SL" is short for scale length, as defined in section 3.5.

We first use the model to examine whether shelf sediments could supply the observed DFe concentrations in surface waters. Throughout this work a horizontal eddy diffusivity of 180–360 m^2 s^{-1} is assumed, scaled for the nearshore region [*Okubo*, 1971; *De Jong et al.*, 2015]. A DFe flux of at least 5000 nmol m^{-2} d^{-1} from the 80 km wide shelf is most consistent with the DFe concentrations observed in shelf surface waters (Figure 8), as a smaller flux does not fit the observed DFe concentrations as well over the shelf (Figure S3). Fluxes this high and higher were inferred from shelf sediments in the Southern Ocean

[*de Jong et al.*, 2012; *De Jong et al.*, 2015]. A scavenging rate constant between 0.003 day^{-1} and 0.016 day^{-1} is required to fit the reduced DFe concentrations offshore (Figure 8). In addition to fitting our data, these rate constants are similar to values invoked in recent Fe models [*Moore and Braucher*, 2008; *Nickelsen et al.*, 2015]. Rate constants at the upper end of this range are required to offset a sediment Fe flux of 10,000 nmol m^2 d^{-1}, while smaller values for rate constants fit the data when the sediment flux is assumed to be 5000 nmol m^{-2} d^{-1} (Figure 8). If the scavenging rate constant is too large, or if the sediment flux is too small, the modeled concentrations of DFe are lower than observed on the shelf (Figures 8 and S3). If the scavenging rate constant is too small, the concentrations of DFe do not decrease as rapidly offshore as observed. The good fit of the data to these simple model simulations confirms that the DFe data can be simulated by a flux of DFe from shelf sediments, horizontal transport by eddy diffusion, and removal by scavenging. The simulations are also consistent with the scale length-derived suggestion that the vast majority of DFe derived from shelf sediments is removed within hundreds of kilometers of the shelf break, suggesting that other sources of DFe (including dust) must be important farther offshore.

The model fits the DFe data without invoking offshore advection that might be expected on the eastern flanks of the Yakutat eddy. Indeed, a modeled offshore current speed expected on the flank of the eddy of ~0.4 m s^{-1} [*Ladd et al.*, 2005b] would carry the high DFe concentrations much farther offshore than observed. This is a conundrum, as the high TDFe concentrations in surface waters of Station 5 in April (Figures 3 and 4 and S1) can only be explained by offshore advection within such an eddy, yet the DFe concentrations decrease offshore much faster than would occur if high-DFe shelf waters were being advected offshore at those speeds. One possible reconciliation of this apparent conflict is that it might take some days for Fe dissolution/desorption from the advected particles to increase the DFe concentrations, and our sampling occurred just after the particles were advected offshore but before much DFe could be solubilized from the particles. Given the westward advection of this eddy at the time of our 7–9 April sampling (see Figure 6a and time series in the supporting information), this explanation seems plausible.

This work shows that DFe data can be modeled assuming that DFe is derived from shelf sediments and that DFe is removed by scavenging assuming first-order rate constants similar to those assumed in state-of-the-art ocean Fe models [*Moore and Braucher*, 2008; *Nickelsen et al.*, 2015]. The consistency of these model results and scale length calculations (reviewed in *Hopwood et al.* [2015]) suggests that little of the shelf-derived DFe is transported more than a hundred kilometers beyond the shelf break. These observations and model interpretation are consistent with all known DFe data from shelf and slope waters of the subarctic NE Pacific [e.g., *Wu et al.*, 2009; *Lippiatt et al.*, 2010; *Aguilar-Islas et al.*, 2016; this work]. Given similar abiological behavior of Th and Fe in the ocean [*Parekh et al.*, 2004; *Moore and Braucher*, 2008] these results are also consistent with the removal of most Th from surface waters within ~300 km of the coast of Fukushima in the NW Pacific [*Hayes et al.*, 2013], inferred from observations of long-lived radium isotopes [*Charette et al.*, 2013]. However, our interpretations differ from some other models assume that only sediment-derived DFe is important to surface waters of the subarctic North Pacific [*Tagliabue et al.*, 2014]. Our work implies that sources of DFe other than resuspended shelf sediments must be important to surface waters well beyond the shelf break. This also implies that iron limitation could be more important in large ocean basins in tectonically active settings, due to narrow continental shelves with spatially limited capacity for offshore propagation of shelf-derived resuspended sediment (e.g., the Pacific), and less common in smaller, geologically older basins with wider continental shelves (e.g., the Arctic and Atlantic oceans). This is consistent with the known locations of some of the largest Fe-limited water bodies, including the subarctic north Pacific and equatorial Pacific oceans. Important sources of DFe beyond the continental shelf break could include dust [*Crusius et al.*, 2011], eddies [*Lippiatt et al.*, 2010; *Xiu et al.*, 2011], icebergs [*Raiswell et al.*, 2006], upwelling [*Bruland et al.*, 2001], hydrothermal sources [*Resing et al.*, 2015], or other possible sources, depending on the location.

While the simulations by this simple sediment-source model fit our DFe data reasonably well, they predict that DFe concentrations will decrease to near zero within a few hundred kilometers of the coast (Figure 8), as was observed in the coastal GoA region by *Wu et al.* [2009] and by *Aguilar-Islas et al.* [2016], and as is suggested by the estimates of the scale length of DFe from high-latitude sites (see section 3.5) [*Hopwood et al.*, 2015]. Although we do not have DFe data from waters more than 50 km beyond the shelf break, dust is known to provide an episodic source of DFe to surface waters far beyond the shelf break, which are

Table 2. Estimates of the Flux of Dust to the Northern GoA Region by Different Methods[a]

Dust Flux (g m^{-2} a^{-1})	Distance From Shore (km)	Data Source	Date of Observations	Reference
0.9–2.6	350	MODIS and CALIPSO satellite aerosol optical depth	November 2006	[*Crusius et al.*, 2011]
~0.7–1.2[b]	300–1000	Water-column ^{230}Th and ^{232}Th measurements	~2008–2009	[*Hayes et al.*, 2013]
~1–2	~600–1000	Core-top ^{230}Th normalization	Centuries-long average	[*Serno et al.*, 2014]

[a]The dust flux observed in *Crusius et al.* [2011] stems primarily from the Copper River and possibly other glacierized river valley sources along the southern Alaska coastline, while the other estimates include all possible dust sources, including Alaskan and Asian sources, and possibly even volcanic ash.
[b]Based on stations SO202-24 and SO202-32 located south of Alaska.

Fe-limited. Dust storms emanating from glacierized river valleys along the northern GoA coastline have been shown to transport dust hundreds of kilometers beyond the shelf break in the late autumn [e.g., *Crusius et al.*, 2011; *Schroth et al.*, 2017], while dust from the Gobi and other deserts have been reported in this region in the spring [*Zdanowicz et al.*, 2006; *Yasunari et al.*, 2007]. The annual dust flux to the eastern subarctic North Pacific ocean has been estimated by several different independent methods to be approximately 1 g m^{-2} a^{-1} (Table 2). Assuming a winter mixed layer depth of 100 m, a dust Fe concentration of 5% by mass, and dissolution or desorption of 10% of the total Fe into seawater soon after deposition [*De Jong et al.*, 2015; *Schroth et al.*, 2009], a dust flux of 1 g m^{-2} that occurs during a brief event during the winter or spring (yielding a DFe flux of ~90 μmol m^{-2} a^{-1}) is sufficient to generate an initial DFe concentration of ~1 nmol kg^{-1} in surface waters. This DFe concentration could be higher if the dust flux was greater, the mixed layer depth was shallower, or if dust solubility was greater than assumed here. For comparison, *Hayes et al.* [2013] assumed a ^{232}Th solubility of 20%. There are very few wintertime DFe concentrations from the GoA region to compare this to, but these calculations suggest that dust is an important source of DFe to GoA surface waters seaward of the shelf.

This suggestion that dust is an important source of DFe to the GoA beyond the shelf break stands in contrast to recent work suggesting dust is less important than other Fe sources throughout the Southern Ocean [e.g., *Raiswell et al.*, 2006; *Gerringa et al.*, 2012; *Borrione et al.*, 2014; *Winton et al.*, 2014; *Wagener et al.*, 2008]. One simple reason for this difference is that the GoA has extensive local sources of dust, as glaciers along the Southern Alaska coastline undergo a melting season lasting months [*Neal et al.*, 2010] that leads to expansive dust source regions along glacierized river valleys [e.g *Crusius et al.*, 2011]. In contrast, Antarctica is far colder, undergoes far less melting of glaciers on land, and therefore has less local dust source material, leading to far lower dust fluxes to the surface of the Southern Ocean [*Borrione et al.*, 2014; *Winton et al.*, 2014; *Wagener et al.*, 2008]. The glaciers along the Antarctic Peninsula extend farther north than the rest of the continent, however, and as that region warms, glacial melt could lead to larger dust source areas, more akin to the sources in Southern Alaska at present.

3.7. Possible Climate Change Impacts

Climate change is impacting many processes that influence the fluxes of both iron and nitrate to GoA surface waters, each of which could influence the marine ecosystem. Air temperature increases have contributed to increased rates of glacier mass loss in southern Alaska in recent years [*Jacob et al.*, 2012; *Arendt et al.*, 2013], with likely increased discharge of Fe-rich waters from the glacierized rivers that dominate the flux of particulate Fe to the northern GoA [*Schroth et al.*, 2011]. However, surface water freshening and warming [e.g., *Freeland et al.*, 1997; *Royer and Grosch*, 2006] have likely led to increased water column stratification throughout the year. This may have reduced sediment resuspension, and the corresponding winter Fe flux to surface waters over the shelf, despite the increased river discharge of Fe, and despite the very large inventory of Fe in shelf sediments. As of 2010, this work shows that there was clearly a large flux of labile particulate Fe to surface waters during the early spring and that this flux did not limit the concentration of DFe over the continental shelf (Figures 3–5). The increased stratification may also be reducing the flux of nitrate to surface waters in the subarctic North Pacific [*Whitney and Freeland*, 1999], although gradual nitrate enrichment below the euphotic zone has been suggested to be countering the impact of increased stratification [*Whitney et al.*, 2013]. Productivity throughout much of the subarctic North Pacific is determined by the flux of the limiting nutrient, Fe, to surface waters, and increased water-column stratification has no effect on atmospheric Fe inputs. More observations are needed to determine whether atmospheric inputs of DFe to the GoA are increasing from dust [e.g., *Crusius et al.*, 2011], as well as from increased coal consumption in China [e.g.,

Le Quéré et al., 2015], given the extremely high solubility of fossil fuel-sourced Fe [*Schroth et al.*, 2009; *Sholkovitz et al.*, 2009]. Increased physical stratification in the GoA, coupled with increased inputs of Fe from atmospheric sources, could lead to increased productivity and a transition from Fe limitation to nitrate limitation, a notion first suggested almost 20 years ago [*Freeland et al.*, 1997].

4. Summary and Conclusions

Dominant source terms in the DFe budget for northern GoA coastal surface waters include mobilization of Fe from resuspended shelf sediment, glacial meltwater, and atmospheric input, all of which may be modulated in response to regional and global climate change. In order to better assess controls on DFe concentrations in the northern GoA, water-column sampling was carried out in 2010 along a transect extending from the mouth of the Copper River to 50 km beyond the continental shelf break. Total dissolvable Fe (TDFe) concentrations were close to 1000 nmol kg^{-1} in April and May in response to sediment resuspension along the shelf, resuspension which was also visible in satellite images. TDFe concentrations over the shelf showed similar maxima in late July but were controlled by entirely different processes, including inputs of low-S meltwater from the Copper River plume and from the Alaska Coastal current, 30–50 km offshore. DFe concentrations in surface waters were surprisingly constant in both April and July, ranging from ~4 nmol kg^{-1} near shore to ~1–2 nmol kg^{-1} at the most offshore sampling site, despite depletion of nitrate over that same timespan, and were far lower than the TDFe concentrations. The nearly constant DFe concentrations along the shelf may be driven by solubilization of resuspended particulate matter by strong Fe-complexing organic ligands, as suggested by previous work, and might be maintained by the high TDFe concentrations that provide a flux of labile Fe during the entire sampling period. The surface water DFe concentrations in April can be simulated for the entire transect using a simple numerical model that assumes a DFe flux from shelf sediments, horizontal transport by eddy diffusion, and removal by scavenging, with rates of all processes within the ranges observed in published work on coastal Fe cycling. However, the model also predicts removal of most of the DFe from the shelf source within a few hundred kilometers of the coast. Calculations suggest that a DFe concentration of ~1 nmol kg^{-1} could be achieved hundreds of kilometers beyond the shelf break from dust deposition, based on published estimates of dust fluxes to surface waters and published rates of dissolution or desorption of DFe from the dust. Given that Fe is the limiting nutrient in the GoA, more work is clearly warranted to understand the processes that control DFe concentrations in Alaskan coastal waters as well as in the GoA. Fluxes from shelf sediments, meltwater, eddies, dust, and fossil fuel combustion could all be important, and all could be changing in response to global change.

Acknowledgments

J.C. and A.W.S. acknowledge the USGS Coastal and Marine Geology Program, the USGS National Climate Change and Wildlife Science Center, and NASA for support. J.T.C. acknowledges the support of Canada's Natural Sciences and Engineering Research Council. We have no financial conflicts of interest. All data from this work, and the numerical model code and simulations, are archived by the USGS at http://doi.org/10.5066/F7222S06. We thank captain Dave Beam of the R/V *Montague* (Cordova, AK), and crew, for careful positioning of the ship, good food, good company, and keeping us out of harm's way. Thanks to Rob Sherrell for sharing his extensive knowledge of trace metal-clean sampling using a towfish. Thanks to Ken Bruland for guidance on shipboard clean lab setup. Thanks to Wally Brooks (USGS), Eva Schemmel, and Blisseth Sy (PWSSC) for sampling help; to Nathan Buck (JISAO) for analytical help; and to Scott Birdwhistell (WHOI) for ICP-MS setup. Thanks to three anonymous reviewers, to Rose Cunningham for the help with the metadata, and to Michael Casso for reviewing the datafiles. The true-color MODIS image in Figure 1 was generated using HDFlook (http://www-loa.univ-lille1.fr/Hdflook/hdflook_gb.html). Figures 2 and 4 were produced using matplotlib (http://matplotlib.org), using a script written in Python [e.g., *Hunter*, 2007] in the Anaconda working environment. This is PMEL publication no. 4531, and JISAO publication no. 2016-1-28. Any use of trade, firm, or product names is for descriptive purposes only and does not imply endorsement by the U.S. Government.

References

Aguilar-Islas, A. M., M. J. M. Séguret, R. Rember, K. N. Buck, P. Proctor, C. W. Mordy, and N. B. Kachel (2016), Temporal variability of reactive iron over the Gulf of Alaska shelf, *Deep Sea Res., Part II*, *15*, 90–106, doi:10.1016/j.dsr2.2015.05.004.

Ardelan, M. V., O. Holm-Hansen, C. D. Hewes, C. S. Reiss, N. S. Silva, H. Dulaiova, E. Steinnes, and E. Sakshaug (2010), Natural iron enrichment around the Antarctic Peninsula in the Southern Ocean, *Biogeosciences*, *7*(1), 11–25.

Arendt, A., S. Luthcke, A. Gardner, S. O'Neel, D. Hill, G. Moholdt, and W. Abdalati (2013), Analysis of a GRACE global mascon solution for Gulf of Alaska glaciers, *J. Glaciol.*, *59*(217), 913–924, doi:10.3189/2013JoG12J197.

Bathen, K. H. (1972), On the seasonal changes in the depth of the mixed layer in the North Pacific Ocean, *J. Geophys. Res.*, *77*, 7138–7150, doi:10.1029/JC077i036p07138.

Borrione, I., O. Aumont, M. C. Nielsdottir, and R. Schlitzer (2014), Sedimentary and atmospheric sources of iron around South Georgia, Southern Ocean: A modelling perspective, *Biogeosciences*, *11*(7), 1981–2001, doi:10.5194/bg-11-1981-2014.

Boyd, P. W., et al. (2004), The decline and fate of an iron-induced subarctic phytoplankton bloom, *Nature*, *428*(6982), 549–553.

Brabets, T. P. (1997), Geomorphology of the lower Copper River, Alaska, *U.S. Geol. Surv. Prof. Pap.*, *1581*, 89 pp.

Brandes, J. A., and A. H. Devol (2002), A global marine-fixed nitrogen isotopic budget: Implications for Holocene nitrogen cycling, *Global Biogeochem. Cycles*, *16*(4), 1120, doi:10.1029/2001GB001856.

Brown, M. T., S. M. Lippiatt, M. C. Lohan, and K. W. Bruland (2012), Trace metal distributions within a Sitka eddy in the northern Gulf of Alaska, *Limnol. Oceanogr.*, *57*(2), 503–518, doi:10.4319/lo.2012.57.2.0503.

Bruland, K. W., K. J. Orians, and J. P. Cowen (1994), Reactive trace metals in the stratified central North Pacific, *Geochim. Cosmchim. Acta*, *58*(15), 3171–3182.

Bruland, K. W., E. L. Rue, and G. J. Smith (2001), Iron and macronutrients in California coastal upwelling regimes: Implications for diatom blooms, *Limnol. Oceanogr.*, *46*(7), 1661–1674.

Bucciarelli, E., S. Blain, and P. Treguer (2001), Iron and manganese in the wake of the Kerguelen Islands (Southern Ocean), *Mar. Chem.*, *73*(1), 21–36, doi:10.1016/s0304-4203(00)00070-0.

Charette, M. A., C. F. Breier, P. B. Henderson, S. M. Pike, I. I. Rypina, S. R. Jayne, and K. O. Buesseler (2013), Radium-based estimates of cesium isotope transport and total direct ocean discharges from the Fukushima nuclear power plant accident, *Biogeosciences*, *10*(3), 2159–2167, doi:10.5194/bg-10-2159-2013.

Chase, Z., P. G. Strutton, and B. Hales (2007), Iron links river runoff and shelf width to phytoplankton biomass along the U.S. West Coast, *Geophys. Res. Lett.*, *34*, L04607, doi:10.1029/2006GL028069.
Childers, A. R., T. E. Whitledge, and D. A. Stockwell (2005), Seasonal and interannual variability in the distribution of nutrients and chlorophyll a across the Gulf of Alaska shelf: 1998–2000, *Deep Sea Res., Part II*, *52*(1–2), 193–216.
Cochran, J. K. (1985), Particle mixing rates in sediments of the eastern equatorial Pacific: Evidence from ^{210}Pb, $^{239+240}$Pu and ^{137}Cs distributions at MANOP sites, *Geochim. Cosmochim. Acta*, *49*, 1195–1210.
Crawford, W. R. (2002), Physical characteristics of Haida eddies, *J. Oceanogr.*, *58*(5), 703–713.
Crawford, W. R., J. Y. Cherniawsky, and M. G. G. Foreman (2000), Multi-year meanders and eddies in the Alaskan Stream as observed by TOPEX/Poseidon altimeter, *Geophys. Res. Lett.*, *27*(7), 1025–1028, doi:10.1029/1999GL002399.
Crawford, W. R., P. J. Brickley, and A. C. Thomas (2007), Mesoscale eddies dominate surface phytoplankton in northern Gulf of Alaska, *Prog. Oceanogr.*, *75*(2), 287–303.
Crusius, J. (1992), Evaluating the mobility of ^{137}Cs, $^{239+240}$Pu and ^{210}Pb from their distributions in laminated sediments, PhD thesis, 253 pp., Columbia Univ., New York.
Crusius, J., A. W. Schroth, S. Gasso, C. M. Moy, R. C. Levy, and M. Gatica (2011), Glacial flour dust storms in the Gulf of Alaska: Hydrologic and meteorological controls and their importance as a source of bioavailable iron, *Geophys. Res. Lett.*, *38*, L06602, doi:10.1029/2010GL046573.
Cullen, J. T., M. Chong, and D. Ianson (2009), British Columbian continental shelf as a source of dissolved iron to the subarctic northeast Pacific Ocean, *Global Biogeochem. Cycles*, *23*, GB4012, doi:10.1029/2008GB003326.
de Jong, J., V. Schoemann, D. Lannuzel, P. Croot, H. de Baar, and J. L. Tison (2012), Natural iron fertilization of the Atlantic sector of the Southern Ocean by continental shelf sources of the Antarctic Peninsula, *J. Geophys. Res.*, *117*, G01029, doi:10.1029/2011JG001679.
De Jong, J. T. M., S. E. Stammerjohn, S. F. Ackley, J.-L. Tison, N. Mattielli, and V. Schoemann (2015), Sources and fluxes of dissolved iron in the Bellingshausen Sea (West Antarctica): The importance of sea ice, icebergs and the continental margin, *Mar. Chem.*, *177*, 518–535, doi:10.1016/j.marchem.2015.08.004.
Ducet, N., P.-Y. Le Traon, and G. Reverdin (2000), Global high resolution mapping of ocean circulation from TOPEX/Poseidon and ERS-1 and -2, *J. Geophys. Res.*, *105*, 19,477–19,498, doi:10.1029/2000JC900063.
Dulaiova, H., M. V. Ardelan, P. B. Henderson, and M. A. Charette (2009), Shelf-derived iron inputs drive biological productivity in the southern Drake Passage, *Global Biogeochem. Cycles*, *23*, GB4014, doi:10.1029/2008GB003406.
Fitzsimmons, J. N., C. T. Hayes, S. N. Al-Subiai, R. F. Zhang, P. L. Morton, R. E. Weisend, F. Ascani, and E. A. Boyle (2015), Daily to decadal variability of size-fractionated iron and iron-binding ligands at the Hawaii Ocean Time-series Station ALOHA, *Geochim. Cosmochim. Acta*, *171*, 303–324, doi:10.1016/j.gca.2015.08.012.
Freeland, H. J., K. L. Denman, C. S. Wong, F. Whitney, and R. Jacques (1997), Evidence of change in the winter mixed layer in the northeast Pacific Ocean, *Deep Sea Res., Part II*, *44*, 2117–2129.
Gerringa, L. J. A., A. C. Alderkamp, P. Laan, C. E. Thuroczy, H. J. W. De Baar, M. M. Mills, G. L. van Dijken, H. van Haren, and K. R. Arrigo (2012), Iron from melting glaciers fuels the phytoplankton blooms in Amundsen Sea (Southern Ocean): Iron biogeochemistry, *Deep Sea Res., Part II*, *71-76*, 16–31, doi:10.1016/j.dsr2.2012.03.007.
Gower, J. F. R., and S. Tabata (Eds.) (1993), *Measurement of Eddy Motion in the North-East Pacific Using the Geosat Altimeter*, pp. 375–383, Seibutsu Kenkyusha, Tokyo.
Hayes, C. T., R. F. Anderson, M. Q. Fleisher, S. Serno, G. Winckler, and R. Gersonde (2013), Quantifying lithogenic inputs to the North Pacific Ocean using the long-lived thorium isotopes, *Earth Planet. Sci. Lett.*, *383*, 16–25, doi:10.1016/j.epsl.2013.09.025.
Hopwood, M. J., S. Bacon, K. Arendt, D. P. Connelly, and P. J. Statham (2015), Glacial meltwater from Greenland is not likely to be an important source of Fe to the North Atlantic, *Biogeochemistry*, *124*, 1–11, doi:10.1007/s10533-015-0091-6.
Hunter, J. D. (2007), Matplotlib: A 2D graphics environment, *Comput. Sci. Eng.*, *9*(3), 90–95, doi:10.5281/zenodo.44579.
Ito, A. (2011), Mega fire emissions in Siberia: Potential supply of bioavailable iron from forests to the ocean, *Biogeosciences*, *8*(6), 1679–1697, doi:10.5194/bg-8-1679-2011.
Jaeger, J. M., C. A. Nittrouer, N. D. Scott, and J. D. Milliman (1998), Sediment accumulation along a glacially impacted mountainous coastline: North-east Gulf of Alaska, *Basin Res.*, *10*(1), 155–173.
Jacob, T., J. Wahr, W. T. Pfeffer, and S. Swenson (2012), Recent contributions of glaciers and ice caps to sea level rise, *Nature*, *482*(7386), 514–518, doi:10.1038/nature10847.
Jeandel, C., and E. H. Oelkers (2015), The influence of terrigenous particulate material dissolution on ocean chemistry and global element cycles, *Chem. Geol.*, *395*, 50–66, doi:10.1016/j.chemgeo.2014.12.001.
Johnson, K. G., R. M. Gordon, and K. H. Coale (1997), What controls dissolved iron concentrations in the world's oceans?, *Mar. Chem.*, *57*, 137–161.
Johnson, W. K., L. A. Miller, N. E. Sutherland, and C. S. Wong (2005), Iron transport by mesoscale Haida eddies in the Gulf of Alaska, *Deep Sea Res., Part II*, *52*(7–8), 933–953.
Jones, M. N. (1984), Nitrate reduction by shaking with cadmium. Alternative to cadmium columns, *Water Res.*, *18*, 643–646.
Kara, A. B., P. A. Rochford, and H. E. Hurlburt (2000), Mixed layer depth variability and barrier layer formation over the North Pacific Ocean, *J. Geophys. Res.*, *105*, 16,783–16,801.
Ladd, C., N. B. Kachel, C. W. Mordy, and P. J. Stabeno (2005a), Observations from a Yakutat eddy in the northern Gulf of Alaska, *J. Geophys. Res.*, *110*, C03003, doi:10.1029/2004JC002710.
Ladd, C., P. Stabeno, and E. D. Cokelet (2005b), A note on cross-shelf exchange in the northern Gulf of Alaska, *Deep Sea Res., Part II*, *52*(5–6), 667–679, doi:10.1016/j.dsr2.2004.12.022.
Le Quéré, C., et al. (2015), Global carbon budget 2014, *Earth Syst. Sci. Data*, *7*(1), 47–85, doi:10.5194/essd-7-47-2015.
Levitus, S. (1982), Climatological atlas of the World Ocean, NOAA Prof. Pap., 13.
Lippiatt, S. M., M. C. Lohan, and K. W. Bruland (2010), The distribution of reactive iron in northern Gulf of Alaska coastal waters, *Mar. Chem.*, *121*(1–4), 187–199.
Lippiatt, S. M., M. T. Brown, M. C. Lohan, and K. W. Bruland (2011), Reactive iron delivery to the Gulf of Alaska via a Kenai eddy, *Deep Sea Res., Part I*, *58*(11), 1091–1102, doi:10.1016/j.dsr.2011.08.005.
Marchetti, A., M. T. Maldonado, E. S. Lane, and P. J. Harrison (2006), Iron requirements of the pennate diatom pseudo-nitzschia: Comparison of oceanic (high-nitrate, low-chlorophyll waters) and coastal species, *Limnol. Oceanogr.*, *51*(5), 2092–2101.
Martin, J. H. (1988), Iron deficiency limits phytoplankton growth in the northeast Pacific subarctic, *Nature*, *331*, 341–343.
Measures, C. I., J. Yuan, and J. A. Resing (1995), Determination of iron in seawater by flow injection analysis using in-line preconcentration and spectrophotometric detection, *Mar. Chem.*, *50*, 3–12.

Moore, J. K., and O. Braucher (2008), Sedimentary and mineral dust sources of dissolved iron to the world ocean, *Biogeosciences*, *5*(3), 631–656.
Neal, E. G., E. Hood, and K. Smikrud (2010), Contribution of glacier runoff to freshwater discharge into the Gulf of Alaska, *Geophys. Res. Lett.*, *37*, L06404, doi:10.1029/2010GL042385.
Nickelsen, L., D. P. Keller, and A. Oschlies (2015), A dynamic marine iron cycle module coupled to the University of Victoria Earth System Model: The Kiel Marine Biogeochemical model 2 for UVic 2.9, *Geosci. Model Dev.*, *8*(5), 1357–1381, doi:10.5194/gmd-8-1357-2015.
Obata, H., H. Karatani, and E. Nakayama (1993), Automated-determination of iron in seawater by chelating resin concentration and chemiluminescence detection, *Anal. Chem.*, *65*(11), 1524–1528, doi:10.1021/ac00059a007.
Oka, E., L. D. Talley, and T. Suga (2007), Temporal variability of winter mixed layer in the mid- to high-latitude North Pacific, *J. Oceanogr.*, *63*, 293–307.
Okkonen, S. R., T. J. Weingartner, S. L. Danielson, D. L. Musgrave, and G. M. Schmidt (2003), Satellite and hydrographic observations of eddy-induced shelf-slope exchange in the northwestern Gulf of Alaska, *J. Geophys. Res.*, *108*(C2), 3033, doi:10.1029/2002JC001342.
Okubo, A. (1971), Oceanic diffusion diagrams, *Deep Sea Res.*, *18*, 789–802.
Palevsky, H. I., F. Ribalet, J. E. Swalwell, C. E. Cosca, E. D. Cokelet, R. A. Feely, E. V. Armbrust, and P. D. Quay (2013), The influence of net community production and phytoplankton community structure on CO_2 uptake in the Gulf of Alaska, *Global Biogeochem. Cycles*, *27*, 664–676, doi:10.1002/gbc.20058.
Parekh, P., M. J. Follows, and E. Boyle (2004), Modeling the global ocean iron cycle, *Global Biogeochem. Cycles*, *18*, GB1002, doi:10.1029/2003GB002061.
Raiswell, R., M. Tranter, L. G. Benning, M. Siegert, R. De'ath, P. Huybrechts, and T. Payne (2006), Contributions from glacially derived sediment to the global iron (oxyhydr) oxide cycle: Implications for iron delivery to the oceans, *Geochim. Cosmochim. Acta*, *70*(11), 2765–2780.
Resing, J. A., P. N. Sedwick, C. R. German, W. J. Jenkins, J. W. Moffett, B. M. Sohst, and A. Tagliabue (2015), Basin-scale transport of hydrothermal dissolved metals across the South Pacific Ocean, *Nature*, *523*(7559), 200–203, doi:10.1038/nature14577.
Rovegno, P. S., C. A. Edwards, and K. W. Bruland (2009), Observations of a Kenai Eddy and a Sitka Eddy in the northern Gulf of Alaska, *J. Geophys. Res.*, *114*, C11012, doi:10.1029/2009JC005451.
Roache, P. J. (1972), On artificial viscosity, *J. Comput. Phys.*, *10*, 351–365.
Royer, T. C. (1979), On the effect of precipitation and runoff on coastal circulation in the Gulf of Alaska, *J. Phys. Oceanogr.*, *9*, 555–563.
Royer, T. C. (1982), Coastal fresh-water discharge in the Northeast Pacific, *J. Geophys. Res.*, *87*, 2017–2021, doi:10.1029/JC087iC03p02017.
Royer, T. C., and C. E. Grosch (2006), Ocean warming and freshening in the northern Gulf of Alaska, *Geophys. Res. Lett.*, *33*, L16605, doi:10.1029/2006GL026767.
Schroth, A. W., J. Crusius, E. R. Sholkovitz, and B. C. Bostick (2009), Iron solubility driven by speciation in dust sources to the ocean, *Nat. Geosci.*, *2*(5), 337–340.
Schroth, A. W., J. Crusius, F. Chever, B. C. Bostick, and O. J. Rouxel (2011), Glacial influence on the geochemistry of riverine iron fluxes to the Gulf of Alaska and effects of deglaciation, *Geophys. Res. Lett.*, *38*, L16605, doi:10.1029/2011GL048367.
Schroth, A. W., J. Crusius, I. Hoyer, and R. Campbell (2014), Estuarine removal of glacial iron and implications for iron fluxes to the ocean, *Geophys. Res. Lett.*, *41*, 3951–3958, doi:10.1002/2014GL060199.
Schroth, A. W., J. Crusius, S. Gassó, C. M. Moy, N. J. Buck, J. A. Resing, and R. W. Campbell (2017), Position of Aleutian Low drives dramatic interannual variability in atmospheric transport of glacial iron to the Gulf of Alaska, *Geophys. Res. Lett.*, doi:10.1002/2017GL073565.
Serno, S., G. Winckler, R. F. Anderson, C. T. Hayes, D. McGee, B. Machalett, H. J. Ren, S. M. Straub, R. Gersonde, and G. H. Haug (2014), Eolian dust input to the subarctic North Pacific, *Earth Planet. Sci. Lett.*, *387*, 252–263, doi:10.1016/j.epsl.2013.11.008.
Sholkovitz, E. R., P. N. Sedwick, and T. M. Church (2009), Influence of anthropogenic combustion emissions on the deposition of soluble aerosol iron to the ocean: Empirical estimates for island sites in the North Atlantic, *Geochim. Cosmochim. Acta*, *73*(14), 3981–4003, doi:10.1016/j.gca.2009.04.029.
Siedlecki, S. A., A. Mahadevan, and D. E. Archer (2012), Mechanism for export of sediment-derived iron in an upwelling regime, *Geophys. Res. Lett.*, *39*, L03601, doi:10.1029/2011GL050366.
Stabeno, P. J., N. A. Bond, A. J. Hermann, N. B. Kachel, C. W. Mordy, and J. E. Overland (2004), Meteorology and oceanography of the northern Gulf of Alaska, *Cont. Shelf Res.*, *24*(7–8), 859–897.
Strom, S. L., M. B. Olson, E. L. Macri, and C. W. Mordy (2006), Cross-shelf gradients in phytoplankton community structure, nutrient utilization, and growth rate in the coastal Gulf of Alaska, *Mar. Ecol. Prog. Ser.*, *328*, 75–92.
Strom, S. L., K. A. Fredrickson, and K. J. Bright (2016), Spring phytoplankton in the eastern coastal Gulf of Alaska: Photosynthesis and production during high and low bloom years, *Deep Sea Res., Part II*, *132*, 107–121, doi:10.1016/j.dsr2.2015.05.003.
Sunda, W. G., and S. A. Huntsman (1995), Iron uptake and growth limitation in oceanic and coastal phytoplankton, *Mar. Chem.*, *50*, 189–206.
Tabata, S. (1982), The anticyclonic, baroclinic eddy off Sitka, Alaska in the Northeast Pacific Ocean, *J. Phys. Oceanogr.*, *12*, 1260–1282.
Tagliabue, A., O. Aumont, and L. Bopp (2014), The impact of different external sources of iron on the global carbon cycle, *Geophys. Res. Lett.*, *41*, 920–926, doi:10.1002/2013GL059059.
Vink, S., E. A. Boyle, C. I. Measures, and J. Yuan (2000), Automated high resolution determination of the trace elements iron and aluminium in the surface ocean using a towed fish coupled to flow injection analysis, *Deep Sea Res., Part I*, *47*(6), 1141–1156.
Wagener, T., C. Guieu, R. Losno, S. Bonnet, and N. Mahowald (2008), Revisiting atmospheric dust export to the Southern Hemisphere ocean: Biogeochemical implications, *Global Biogeochem. Cycles*, *22*, GB2006, doi:10.1029/2007GB002984.
Wang, J., M. B. Jin, D. L. Musgrave, and M. Ikeda (2004), A hydrological digital elevation model for freshwater discharge into the Gulf of Alaska, *J. Geophys. Res.*, *109*, C07009, doi:10.1029/2002JC001430.
Ware, D. M., and R. E. Thomson (2005), Bottom-up ecosystem trophic dynamics determine fish production in the northeast Pacific, *Science*, *308*(5726), 1280–1284.
Whitney, F. A., and H. J. Freeland (1999), Variability in upper-ocean water properties in the NE Pacific Ocean, *Deep Sea Res., Part II*, *46*(11–12), 2351–2370.
Whitney, F. A., S. J. Bograd, and T. Ono (2013), Nutrient enrichment of the subarctic Pacific Ocean pycnocline, *Geophys. Res. Lett.*, *40*, 2200–2205, doi:10.1002/grl.50439.
Winton, V. H. L., G. B. Dunbar, N. A. N. Bertler, M. A. Millet, B. Delmonte, C. B. Atkins, J. M. Chewings, and P. Andersson (2014), The contribution of aeolian sand and dust to iron fertilization of phytoplankton blooms in southwestern Ross Sea, Antarctica, *Global Biogeochem. Cycles*, *28*, 423–436, doi:10.1002/2013GB004574.
Wu, J., and G. W. Luther III (1996), Spatial and temporal distribution of iron in the surface water of the northwestern Atlantic Ocean, *Geochim. Cosmochim. Acta*, *60*(15), 2729–2741.
Wu, J. F., A. Aguilar-Islas, R. Rember, T. Weingartner, S. Danielson, and T. Whitledge (2009), Size-fractionated iron distribution on the northern Gulf of Alaska, *Geophys. Res. Lett.*, *36*, L11606, doi:10.1029/2009GL038304.

Xiu, P., A. P. Palacz, F. Chai, E. G. Roy, and M. L. Wells (2011), Iron flux induced by Haida eddies in the Gulf of Alaska, *Geophys. Res. Lett.*, *38*, L13607, doi:10.1029/2011GL047946.

Yasunari, T. J., T. Shiraiwa, S. Kanamori, Y. Fujii, M. Igarashi, K. Yamazaki, C. S. Benson, and T. Hondoh (2007), Intra-annual variations in atmospheric dust and tritium in the North Pacific region detected from an ice core from Mount Wrangell, Alaska, *J. Geophys. Res.*, *112*, D10208, doi:10.1029/2006JD008121.

Zdanowicz, C., G. Hall, J. Vaive, Y. Amelin, J. Percival, I. Girard, P. Biscaye, and A. Bory (2006), Asian dustfall in the St. Elias Mountains, Yukon, Canada, *Geochim. Cosmochim. Acta*, *70*(14), 3493–3507.